Research Article | Vol. 30, No. 13 / 20 Jun 2022 / Optics Express 23417
Optics EXPRESS

Light management in ultra-thin photonic power converters for 1310 nm laser illumination

NEDA NOURI,[1,2,*] CHRISTOPHER E. VALDIVIA,[1,2] MEGHAN N. BEATTIE,[1,3] JACOB J. KRICH,[1,2,3] AND KARIN HINZER[1,2,3]

[1]SUNLAB, Centre for Research in Photonics, University of Ottawa, Ottawa, Ontario, K1N 6N5, Canada
[2]School of Electrical Engineering and Computer Science, University of Ottawa, Ottawa, Ontario, K1N 6N5, Canada
[3]Department of Physics, University of Ottawa, Ottawa, Ontario, K1N 6N5, Canada
*nnouri@ottawa.ca

Abstract: We designed and optimized ultra-thin single junction InAlGaAs photonic power converters (PPC) with integrated back reflectors (BR) for operation at the telecommunications wavelength of 1310 nm and numerically studied the light trapping capability of three BR types: planar, cubic nano-textured, and pyramidal nano-textured. The PPC and BR geometries were optimized to absorb a fixed percentage of the incident light at the target wavelength by coupling finite difference time-domain (FDTD) calculations with a particle swarm optimization. With 90% absorptance, opto-electrical simulations revealed that ultra-thin PPCs with 5.6- to 8.4-fold thinner absorber layers can have open circuit voltages (V_{oc}) that are 9-12% larger and power conversion efficiencies (PCE) that are 9-10% (relative) larger than conventional thick PPCs. Compared to a thick PPC with 98% absorptance, these ultra-thin designs reduce the absorber layer thickness by 9.5-14.2 times while improving the V_{oc} by 12-14% and resulting in a relative PCE enhancement of 3-4%. Of the studied BR designs, pyramidal BRs exhibit the highest performance for ultra-thin designs, reaching an efficiency of 43.2% with 90% absorptance, demonstrating the superior light trapping capability relative to planar and cubic nano-textured BRs.

1. Introduction

Already well-known for its revolutionary role in high-speed data transmission, optical fiber has demonstrated significant potential for optical power transmission applications in recent years. Electromagnetic interference immunity, galvanic isolation, and reduced fire hazard make optical fiber a safe and reliable power transmission alternative for driving sensors and low power electronics in hazardous and extreme environments such as high voltage lines, wind turbines, mines, and magnetic resonance imaging [1–4]. Besides power over fiber, free space optical power transmission (power beaming) has also gained attention for a wide range of applications. Some of these applications include remote, wireless powering of equipment such as medical implants [5,6] or aerial vehicles [7] and power beaming to remote locations or between satellites and terrestrial transmitters/receivers [8].

Photonic power converters (PPC) are one of the main components in optical power transmission systems, converting photonic power in the form of narrow-bandwidth light from a laser or LED source into electrical power via the photovoltaic effect. To boost the output voltage to meet application requirements, PPCs can be designed as devices with a single pn junction and combined with conventional DC-DC converters [9] or as stand-alone multi-junction devices, which directly output voltages that scale linearly with the number of series-connected pn junctions [10]. In both cases, the ability of the PPC to absorb the majority of incident irradiance is critical to achieve high optical-to-electrical power conversion efficiency, for applications ranging from milliwatts to tens of watts per chip. As transmittance decreases exponentially with active layer thickness, fulfilling high absorptance requirements (≥ 90% of incoming light) typically requires absorber

#459680 https://doi.org/10.1364/OE.459680
Journal © 2022 Received 5 Apr 2022; revised 3 Jun 2022; accepted 4 Jun 2022; published 13 Jun 2022

Optics EXPRESS

layers with thicknesses of at least several micrometers, leading to slow epitaxial growth and higher material usage. An alternative solution is to reduce the absorber thickness while applying light management techniques to compensate for the reduced absorptance. Thin devices also benefit from higher open circuit voltages (V_{oc}) compared to thick devices due to increased carrier concentration and reduced recombination [11]. Their operation is less sensitive to bulk defects and diffusion length [12]. An added benefit of thin devices is their enhanced power to weight ratio, flexibility, and superior radiation tolerance, which are critical for aerospace applications [13,14].

The majority of commercially available high-efficiency PPCs are based on GaAs absorbers, operating in the range of 800-850 nm wavelengths [15,16]. The optical fiber attenuation loss at these wavelengths is ~3 dB/km (50% per kilometer) which limits use of these devices to short-distance power-over-fiber transmission. Longer wavelengths can significantly extend this reach but require lower bandgap absorbers for which bandgap-voltage offsets represent a greater relative loss, resulting in lower expected maximum optical-to-electrical conversion efficiencies. Nevertheless, this study focuses on the O-band telecommunications window near 1310 nm which provides much lower optical fiber attenuation loss of ~0.5 dB/km (11% per kilometer), resulting in potential for higher total system transmission efficiency in longer-reach future photonic power systems [17–19].

The efficiency of thin PPCs is expected to exceed that of their optically thick counterparts when high absorptance can be maintained through efficient light trapping. Numerous light harvesting strategies have been exploited for high-efficiency thin and ultra-thin solar cells including metal nanoparticles [20,21], photonic crystals and gratings [22,23], nanopyramids [24,25], nanocones [26], nanowires [27], planar or patterned metal back reflectors [28–30], or combinations thereof [31]. Among these methods, front surface texturing alone or in combination with a rear mirror is common. Besides trapping light, front surface texturing can decrease reflection losses across the broad solar spectrum. In the case of PPCs illuminated by narrow-band light, however, near-zero reflection losses can be obtained using a back mirror by appropriately designing the optical cavity formed by the PPC layers. Additionally, back reflectors (BR) can increase the V_{oc} through photon recycling [32].

In this work, we applied numerical simulations to optimize ultra-thin PPC designs under narrow-band laser illumination of 1310 nm using the light trapping capability of flat BR and nanotextured BR with cubic and pyramidal structures.

2. Design

In designing PPCs, selection of the absorber material is a main consideration. Minimizing the difference between the bandgap and the incoming photon energy (0.946 eV, 1310 nm) reduces the thermalization loss, however it also reduces the absorption coefficient. Device layers should all be lattice matched to the substrate (InP) to reduce strain-induced defects that degrade cell performance by acting as recombination centers. We balanced the tradeoff between thermalization losses and absorption coefficient while satisfying the lattice matching constraint by using the quaternary alloy $In_{0.532}Al_{0.097}Ga_{0.371}As$ with a band gap of 0.88 eV for the absorber material in the pn junctions layers [33]. Assuming Beer-Lambert absorptance using a measured absorption coefficient of 7424 cm^{-1} [33], this material requires ~5.3 μm thickness to absorb 98% of the incident light at a 1310-nm wavelength.

Our modeled PPCs consist of the pn junction absorber, surrounded by transparent front and back surface field (FSF and BSF) layers composed of a wider bandgap alloy, $In_{0.527}Al_{0.356}Ga_{0.117}As$ (1.25 eV). Gold, which is highly reflective at the target wavelength, serves as both the back contact and the BR. Figure 1 illustrates the epitaxial structure and back-reflector designs proposed to enable ultra-thin PPCs using flat, cubic and pyramidal textures. In our models, texturing of the

Optics EXPRESS

absorber layers was avoided; although it has been shown to boost optical absorptance, it also degrades electrical performance due to increased surface recombination [31,34].

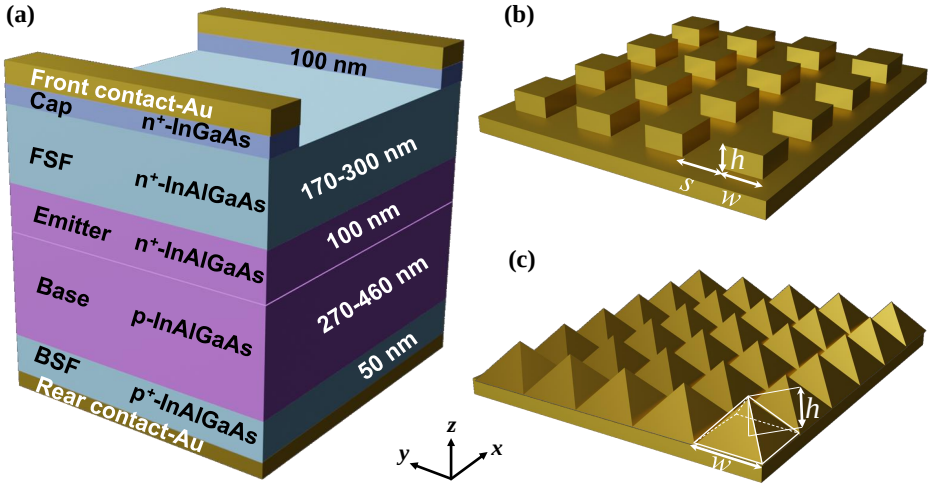

Fig. 1. (a) Schematic structure of ultra-thin PPCs with flat back reflector. Layer thicknesses indicate the range over which each layer was optimized. Illustrations of (b) cubic back reflector with parameters for the height h, width w, and spacing s indicated, and (c) pyramidal back reflector with height h and base width w indicated.

While this paper focuses on numerical simulation, these PPC designs could be realized, for example, by inverted epitaxial growth on the InP substrate. Following epitaxy, the BR could be deposited by blanket metallization or periodic nano-texturing via nanoimprinting (see [34], for example) on the BSF layer. The sample would then be bonded to a mechanical handle, and the InP substrate would be removed through chemical etching or epitaxial liftoff.

3. Simulation and optimization

Optical simulations of PPC devices were performed in the Lumerical FDTD Solutions software using the finite difference time-domain (FDTD) method. The quaternary alloys were modeled with refractive index parameters that were extracted experimentally by ellipsometry measurements of samples with the same composition grown by molecular beam epitaxy [35]. The optical properties of gold (Au) and InP were taken from Palik [36]. The modelled structures were illuminated by a normally incident uniform light with an intensity of 100 mW/cm^2. The laser spectrum featured a Gaussian distribution centered at 1310 nm with a full-width-at-half-maximum linewidth of 10 nm. We performed 2D optical simulations for flat BR designs and 3D optical simulations for textured BR designs over a single unit cell. Periodic and perfectly matched layer (PML) boundary conditions were applied for the lateral (x and y) and growth (z) directions, respectively. For 3D simulations, since both incident light and nanostructures were symmetric with respect to the center of the simulation region in x and y directions, symmetric and antisymmetric boundary conditions also were implemented to reduce computational requirements by reducing simulations to one-quarter of the original simulation area. Pyramids were modelled using a staircase approximation, replacing the pyramid by a series of stacked squares, each diminishing in size and each of 2.5 nm thickness [37], which we confirmed converges J_{ph} to within ±0.3%.

Optics EXPRESS

The PPC's generation rate G was calculated assuming that each absorbed photon generates an electron-hole pair. The total generation rate was calculated by integrating over the linewidth of the laser source as:

$$G(r) = \int P_{\text{abs}}(\lambda.r)\frac{\lambda}{hc}d\lambda \tag{1}$$

where P_{abs} is the absorbed power per volume per wavelength λ and position r, h is Planck's constant, and c is the speed of light in vacuum. The best-case scenario is that all photoexcited carriers are collected at the contacts without any recombination loss, so that the ideal photocurrent density is defined as:

$$J_{\text{ph}} = q \int G(r)dr \tag{2}$$

where q is the elementary charge.

For each BR type, our design optimization sought to minimize the absorber layer thickness while obtaining a target absorptance of 90%, corresponding to a J_{ph} of ~95 mA/cm^2 and a responsivity of 0.95 A/W. Fabry-Perot resonances were aligned to the target wavelength by tuning the optical cavity design, minimizing reflectance and maximizing absorptance. Structure optimization varied the absorber and FSF layer thicknesses for the planar BR design. For the nanotextured BR designs, their geometrical parameters were added to the design space, comprising height h, width w, and spacing s for the cubic BR (Fig. 1(b)), and height h and base width w for the pyramidal BR (Fig. 1(c)). To avoid polarization dependence for normal incidence, nanostructure dimensions were kept equal in the x and y directions. In all cases, the BSF layer thickness was fixed at 50 nm. These parameter spaces were investigated via a particle swarm algorithm [38], using photocurrent J_{ph} as the figure of merit.

We simulated two thick PPCs on InP substrates to use as baselines to compare the light harvesting capability and power conversion efficiencies of ultra-thin PPCs. One of the thick PPCs was simulated with high (98%) absorptance and the other with same absorptance (90%) as the optimized ultra-thin devices. The required absorber thicknesses are 5270 nm and 3100 nm for the 98% and 90% designs, respectively. Without an antireflection coating, both thick designs would suffer from ~30% reflection loss. To achieve a fair comparison with ultra-thin designs which benefit from near-zero reflection loss, the FSF layer thickness was optimized in conjunction with a double-layer antireflection coating (ARC) of SiO_2/TiO_2 [39] in the thick PPC designs. We refer to these designs as Ref 98% and Ref 90%.

For these optically thick designs, the J_{ph} values obtained from simulations were about 0.02 mA/cm^2 lower than analytical calculations according to:

$$J_{\text{ph,th}} = \frac{qAP}{E_{\text{ph}}} \tag{3}$$

where $J_{\text{ph,th}}$ is the theoretical photocurrent, A is the absorptance, P is the input power, and E_{ph} is the energy of the incident photon.

For further verification of optical simulations, we compared the model performance to a fabricated device with a 4100 nm absorber layer thickness, corresponding to 95% absorptance. The close match between the experimental measurements and simulation results for the reflectance spectra is shown in Appendix B.

After optimization of devices structures through optical simulations, we conducted electrical simulations to evaluate device performance. The model included: bulk recombination losses – radiative, Shockley-Read-Hall (SRH), and Auger; 5% gridline shading loss; and ideal ohmic contacts with no contact resistance. Electrical simulations were performed using the finite element drift-diffusion method using the charge transport simulator, CHARGE by Lumerical, applying a device temperature of 300K. The generation rate G obtained from the optical simulations was used as input for the electrical simulations. Except for SRH carrier lifetime and bandgap, other material parameters for the quaternary alloy $In_xAl_yGa_{1-x-y}As$ were determined by interpolation

Optics EXPRESS

between the three ternary constituents: GaInAs, AlInAs, and AlGaAs [40,41]. Some of these parameters for the active layer are given in Appendix A. SRH carrier lifetime depends significantly on the material and growth quality and could vary from microseconds to picoseconds. For these simulations we selected 100 ns to represent high quality material. See Appendix B for comparison of the experimentally measured and simulated *I-V* curves for a fabricated device with 4100 nm absorber layer thickness.

4. Results and discussion

Table 1 reports the optimized design parameters with corresponding absorptance and primary optical losses including parasitic absorption in the back mirror and reflectance. For BR designs, near-zero reflection loss was obtained without the incorporation of an ARC. Reflection spectra for all five designs from Table 1 are shown in Fig. 2.

Table 1. Optimized parameters of PPCs with corresponding absorptance and optical losses at 1310 nm.

	Ref 98%	Ref 90%	Flat	Cubic	Pyramidal
ARC 2 (nm)	180	206	-	-	-
ARC 1 (nm)	94	122	-	-	-
FSF (nm)	214	299	240	300	170
Absorber (nm)	5270	3100	557	410	371
w (nm)	-	-	-	290	653
s (nm)	-	-	-	430	-
h (nm)	-	-	-	93	108
Absorptance (%)	97.97	89.99	90.32	90.57	90.31
Reflectance (%)	0.03	0.01	2.38	0.01	0.04
Back reflector loss (%)	-	-	7.30	9.42	9.65

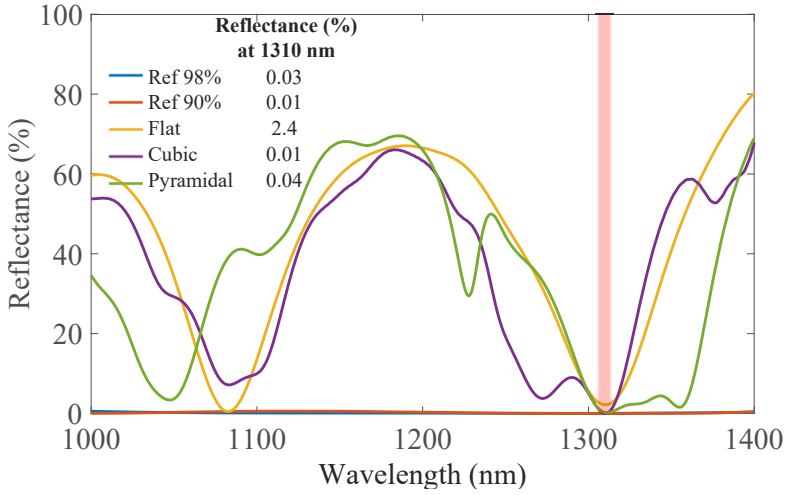

Fig. 2. Reflection spectrum versus wavelength for all five optimized PPC designs, including optically thick (Ref 98%, Ref 90%) and ultra-thin (flat, cubic, and pyramidal back-reflectors). These designs were optimized for near zero reflection loss at 1310 nm wavelength. The laser spectrum centered at 1310 nm is indicated by the vertical line.

Optics EXPRESS

The cross-sectional absorbed power profiles and corresponding J_{ph} values are depicted in Fig. 3 for all five structures: Ref 98%, Ref 90%, flat, cubic, and pyramidal BRs. For the thick reference PPCs, shown in Figs. 3(a),(b), most of the light absorption occurs near the front surface and decreases as less light penetrates deeper into the absorbing layer, as expected. However, for the ultra-thin planar structure in Fig. 3(c) and nano-textured structures in Figs. 3(d),(e), the back mirrors create strong Fabry-Perot resonances in the absorptance profiles. Additionally, the nano-textured back mirrors also induce guided mode resonances that further enhance light trapping at the resonance wavelength. The 625-nm thick InP substrates of the reference designs are not fully depicted in Fig. 3, although they were included in the simulations. The J_{ph} values are close to 95 mA/cm^2 for the flat, cubic and pyramidal BR designs, indicating that they each absorb approximately 90% of the incident light despite reducing the absorber thickness by 5.6, 7.6, and 8.4 times, respectively, relative to the Ref 90% structure. Compared to Ref 98%, flat, cubic and pyramidal structures achieve 9.5-, 12.5- and 14.2-fold reductions in the absorber layer thickness.

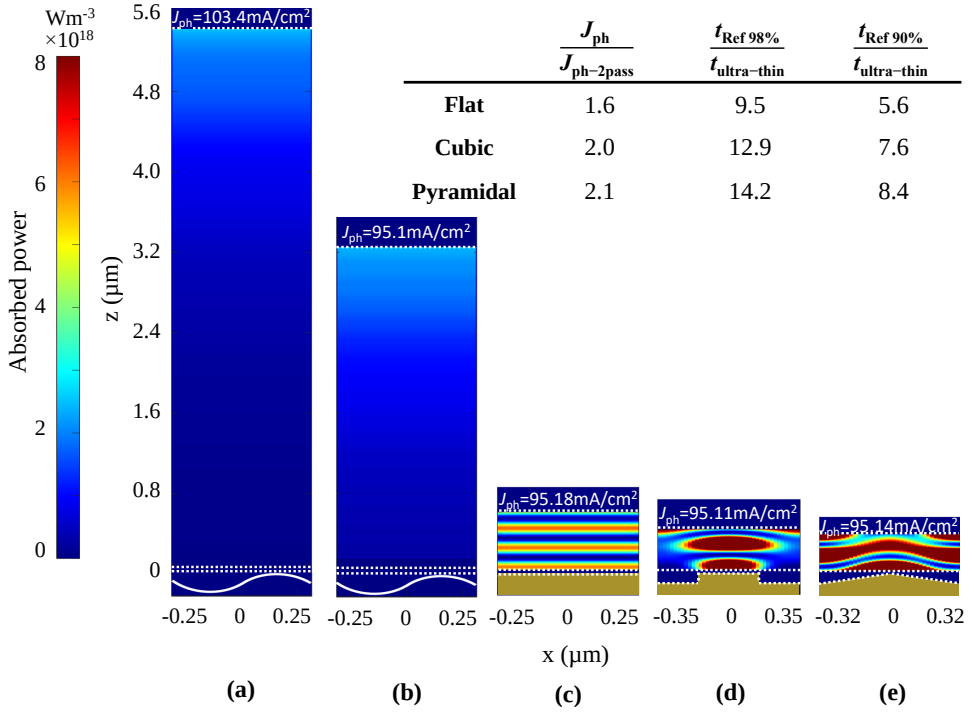

	$\frac{J_{ph}}{J_{ph-2pass}}$	$\frac{t_{Ref\ 98\%}}{t_{ultra-thin}}$	$\frac{t_{Ref\ 90\%}}{t_{ultra-thin}}$
Flat	1.6	9.5	5.6
Cubic	2.0	12.9	7.6
Pyramidal	2.1	14.2	8.4

Fig. 3. Cross-sectional absorbed power profiles at $y = 0$ of each optimized PPC design: (a) Ref 98%, (b) Ref 90%, (c) flat, (d) cubic, and (e) pyramidal BRs. Inset table compares light trapping capability and thickness reduction of proposed PPCs (t: absorber thickness). Note that the x scales differ for each (d) and (e) compared to (a)-(c). The dotted white lines indicate material interfaces. The FSF and BSF, above and below the absorber, are transparent to the incident light. Only a small portion of the substrate is shown in (a) and (b), as indicated by the wavy lines.

The light-trapping ability of a thin structure can be quantified by comparing it to the Beer-Lambert absorption through a material with twice its thickness. This emulates the expected absorption by two passes through the structure, assuming a perfect back reflector and no additional reflections or scattering. This two-pass photocurrent, $J_{ph-2pass}$, is calculated by Eq. (3) with A set as the Beer-Lambert absorptance for twice the absorber thickness of the corresponding

Optics EXPRESS

design. In the ultra-thin designs, optical cavity and guided-mode resonances result in simulated photocurrents that are enhanced by factors of 1.6, 2.0, and 2.1 for the flat, cubic, and pyramidal BRs, respectively, in comparison to the two-pass case. The pyramidal BR design has the most significant reduction in absorber thickness, demonstrating its greater light scattering and trapping capability compared to planar and cubic nano-textured BRs.

The designs proposed here were optimized to minimize the absorber layer thickness while retaining 90% absorptance. However, alternative designs can also achieve nearly 90% absorptance with slightly (30-50 nm) thicker absorber layers using a different combination of design parameters such as FSF thickness and/or nanotexture dimensions [42,43]. Therefore, allowing a slightly thicker absorber can broaden the design freedom significantly.

The reflectance spectrum and resonance linewidth differ significantly between thin PPC designs (Fig. 2). For optical power transmission applications, resonances with wider linewidths are desired, as the operating wavelength of a laser can deviate due to manufacturing tolerances or temperature fluctuations [44], and performance can be affected by other conditions such as illumination angle. Although we simulated near-zero reflection loss (Fig. 2) without incorporating an ARC, applying an ARC could increase the resonance linewidth and minimize reflection over a larger spectral range, improving the stability and applicability of these devices. Such an ARC would also affect the optimum thickness of other layers due to interference effects and expand the design freedom.

Current-voltage characteristics and device efficiencies obtained from electrical simulations (Fig. 4) show that the ultra-thin designs with planar and textured back reflectors improve the V_{oc} by 12-14% and the power conversion efficiency (PCE) by 3-4% (relative), as compared to the Ref 98% design. In comparison with the Ref 90% design, the optimized ultra-thin designs match the J_{sc}, boost the V_{oc} by 9-12%, and increase the PCE by 9-10% (relative). The higher efficiency in ultra-thin designs is caused by the increased open-circuit voltage, which is enabled by the strong light-trapping induced by the back reflectors.

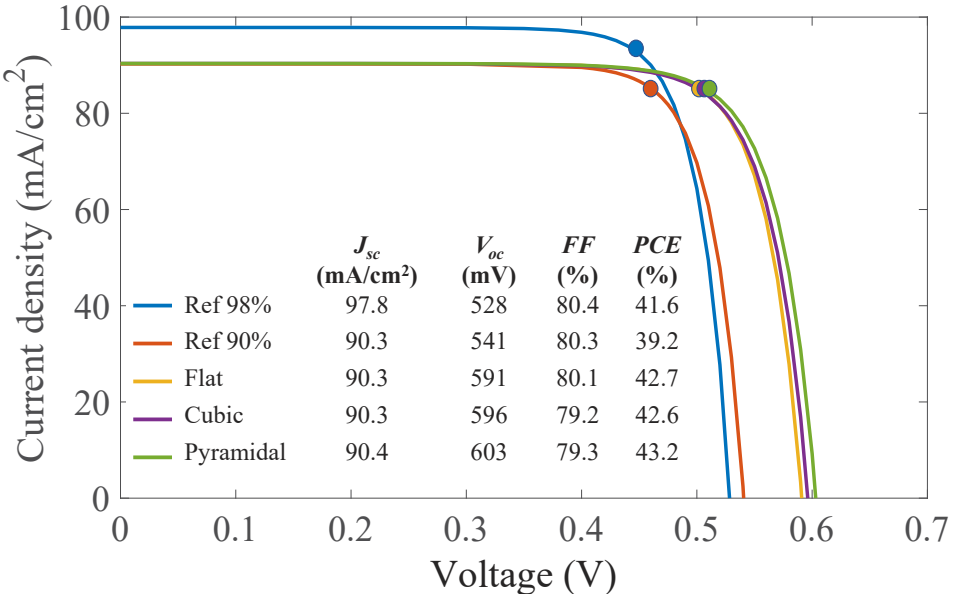

Fig. 4. Current-voltage characteristics of the proposed PPCs under intensity of 100 mW/cm^2 at T=300K. Maximum power points are indicated by the colored circles.

Optics EXPRESS

The main parasitic optical loss for the ultra-thin PPCs is absorption in the back mirror [45], as shown in Table 1, which is worse for the textured structures that have more light trapping and thus more interaction between light and the back surface. The main electrical loss can be due to SRH carrier lifetime, which varies over orders of magnitude depending on the material quality. For example, for pyramidal nanotextured BR structures, an SRH lifetime in the InAlGaAs absorber layer of 10, 100, and 1000 ns results in efficiencies of 35%, 43.2%, and 46% [46], respectively. Real-world devices may include additional losses such as those from surface recombination and thermal effects.

By increasing the illumination intensity to 10 W/cm^2, the simulated efficiencies of the Ref 98% and pyramidal nanotextured BR designs increased to 50.5% and 56.2%, respectively. The simulated efficiencies of the Ref 98% device under both these low and high intensities are the same as those observed experimentally for the optically thick PPCs of Ref [18]. Further efficiency improvements could be achieved by shifting the absorber bandgap closer to the incident photon energy to reduce the thermalization loss [47], optimizing the front metallization [48], and employing higher quality material with longer carrier lifetimes. These simulations did not account for photon recycling effects, which would yield higher efficiencies in highly luminescent materials [49,50].

5. Conclusions

In this work, we presented design, simulation, and optimization of light management in highly efficient ultra-thin PPCs, comparing the simulated performance of flat, cubic, and pyramidal nano-textured BRs under 1310 nm narrow-band illumination. Due to strong Fabry-Perot and guided mode back-reflector induced resonances, we attained near-zero reflection loss in the ultra-thin PPCs without applying an antireflection coating. Compared to conventional thick PPCs on a substrate, modelled ultra-thin PPCs with BRs demonstrated superior performance with larger V_{oc} and PCE. The best performance was exhibited by the device with a pyramidal nano-textured BR. Further design optimization, reduced thermalization loss, front metallization engineering, higher intensity laser illumination, and accounting for photon recycling could lead to simulated efficiencies over 50%. The approach proposed here could be applied to other illumination wavelengths and both single and multi-junction PPCs could benefit from these design principles.

Appendix A: Electrical simulation parameters

Table 2 lists some of the parameters of the active layer used in the electrical simulations. The properties for ternary alloys were extracted from [51–53], then linearly interpolated to determine values for the quaternary alloys.

Table 2. Electrical parameters of the absorber layer at T=300K

Parameter	Unit	Value	
		Electrons	Holes
Mobility (μ)	cm^2/Vs	14800	340
Radiative recombination coefficient (B)	cm^3/s	1×10^{-10}	1×10^{-10}
Auger recombination coefficient (C)	cm^6/s	4.9×10^{-29}	4.9×10^{-29}

Appendix B: Experimental measurement and simulation comparison

To demonstrate the accuracy of the simulation, we compared the model performance to a fabricated device with a 4100 nm absorber layer thickness, corresponding to 95% absorptance. As shown in the inset of Fig. 5, the model represents experimentally measured reflectance spectra.

Optics EXPRESS

For reproducing the experimentally measured *I-V* curve, the SRH electron and hole lifetimes were reduced to 1 and 0.1 ns, respectively and band gap narrowing effects were added to the simulations. The lower efficiency of the fabricated device originates from 30% reflection loss, 8% grid line shading, and shorter carrier lifetimes. To highlight the effect of material quality on the PPC's performance, simulations with longer SRH carrier lifetimes (10 ns for both electron and holes) were included in the simulations depicted using a yellow dashed line.

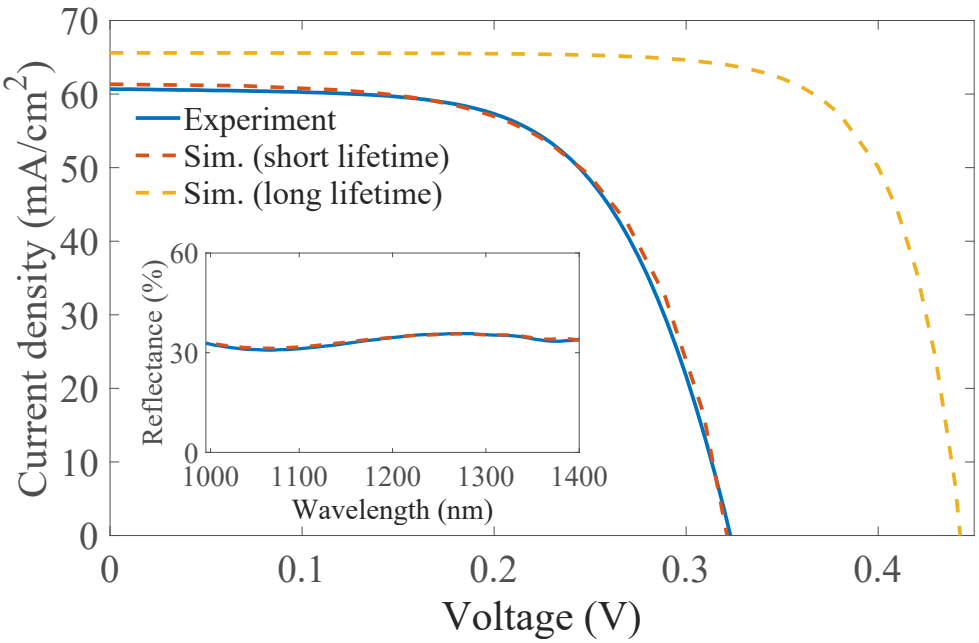

Fig. 5. Experimentally measured and simulated *I-V* curve for a thick PPC with 4100 nm absorber layer thickness under 1310 nm illumination at intensity of 100 mW/cm^2 at T=300K. Inset shows simulated and measured reflectance spectra.

Funding. Natural Sciences and Engineering Research Council of Canada (497981).

Disclosures. The authors declare no conflicts of interest.

Data availability. Data underlying the results presented in this paper are not publicly available at this time but may be obtained from the authors upon reasonable request.

References

1. J. B. Rosolem, *Power-Over-Fiber Applications for Telecommunications and for Electric Utilities* (IntechOpen, 2017).
2. K. Worms, C. Klamouris, F. Wegh, L. Meder, D. Volkmer, S. P. Philipps, S. K. Reichmuth, H. Helmers, A. Kunadt, J. Vourvoulakis, A. W. Bett, C. Koos, W. Freude, J. Leuthold, and W. Stork, "Reliable and lightning-safe monitoring of wind turbine rotor blades using optically powered sensors," Wind Energ. **20**(2), 345–360 (2017).
3. M. M. Wilkins, M. Ishigaki, P.-O. Provost, D. Masson, S. Fafard, C. E. Valdivia, E. M. Dede, and K. Hinzer, "Ripple-Free Boost-Mode Power Supply Using Photonic Power Conversion," IEEE Trans. Power Electron. **34**(2), 1054–1064 (2019).
4. J. G. Werthen, M. J. Cohen, T.-C. Wu, and S. Widjaja, "Electrically Isolated Power Delivery for MRI Applications," in *Proc. Int. Soc. Magn. Reson. Med. Annu. Meeting* (2006), p. 1353.
5. M. Schauerte, O. Höhn, T. Wierzkowski, G. Keller, and H. Helmers, "4-Junction GaAs Based Thin Film Photonic Power Converter with Back Surface Reflector for Medical Applications," in *2021 IEEE 48th Photovoltaic Specialists Conference (PVSC)* (2021), pp. 1954–1959.
6. C. Algora and R. Peña, "Recharging the Battery of Implantable Biomedical Devices by Light," Artif. Organs **33**(10), 855–860 (2009).
7. https://powerlighttech.com/autonomous-vehicles

Optics EXPRESS

8. L. Summerer and O. Purcell, *Concepts for Wireless Energy Transmission via Laser* (Technical Report, Eur. Space Agency, 2009), p. 10.
9. H. Helmers, C. Armbruster, M. von Ravenstein, D. Derix, and C. Schöner, "6-W Optical Power Link With Integrated Optical Data Transmission," IEEE Trans. Power Electron. **35**(8), 7904–7909 (2020).
10. S. Fafard, M. C. A. York, F. Proulx, C. E. Valdivia, M. M. Wilkins, R. Arès, V. Aimez, K. Hinzer, and D. P. Masson, "Ultrahigh efficiencies in vertical epitaxial heterostructure architectures," Appl. Phys. Lett. **108**(7), 071101 (2016).
11. B. M. Kayes, H. Nie, R. Twist, S. G. Spruytte, F. Reinhardt, I. C. Kizilyalli, and G. S. Higashi, "27.6% Conversion efficiency, a new record for single-junction solar cells under 1 sun illumination," in *2011 37th IEEE Photovoltaic Specialists Conference (2011)*, pp. 000004–000008.
12. R. Saive, "Light trapping in thin silicon solar cells: A review on fundamentals and technologies," Prog. Photovolt: Res. Appl. **29**(10), 1125–1137 (2021).
13. F. Cappelluti, G. Ghione, M. Gioannini, G. Bauhuis, P. Mulder, J. Schermer, M. Cimino, G. Gervasio, G. Bissels, E. Katsia, T. Aho, T. Niemi, M. Guina, D. Kim, J. Wu, and H. Liu, "Novel Concepts for High-Efficiency Lightweight Space Solar Cells," E3S Web Conf. **16**, 03007 (2017).
14. L. C. Hirst, M. K. Yakes, J. H. Warner, M. F. Bennett, K. J. Schmieder, R. J. Walters, and P. P. Jenkins, "Intrinsic radiation tolerance of ultra-thin GaAs solar cells," Appl. Phys. Lett. **109**(3), 033908 (2016).
15. S. Fafard, F. Proulx, M. C. A. York, L. S. Richard, P. O. Provost, R. Arès, V. Aimez, and D. P. Masson, "High-photovoltage GaAs vertical epitaxial monolithic heterostructures with 20 thin p/n junctions and a conversion efficiency of 60%," Appl. Phys. Lett. **109**(13), 131107 (2016).
16. S. Fafard and D. P. Masson, "Perspective on photovoltaic optical power converters," J. Appl. Phys. **130**(16), 160901 (2021).
17. M. N. Beattie and K. Hinzer, "Extending the reach of photonic power," Compd. Semicond. **25**, 56–63 (2019).
18. H. Helmers, A. Franke, D. Lackner, O. Höhn, F. Predan, and F. Dimroth, "51% Efficient Photonic Power Converters for O-Band Wavelengths around 1310 nm," in *2020 47th IEEE Photovoltaic Specialists Conference (PVSC)* (2020), pp. 2471–2474.
19. M. Beattie, H. Helmers, C. E. Valdivia, D. Lackner, O. Höhn, and K. Hinzer, "Non-Uniform Illumination Impacts on O-Band InGaAsP and Metamorphic GaInAs Photonic Power Converters," in *3rd Optical Wireless and Fiber Power Transmission Conference, OWPT 2021. Technical Digest* (2021), pp. 37–38.
20. K. R. Catchpole and A. Polman, "Plasmonic solar cells," Opt. Express **16**(26), 21793–21800 (2008).
21. S. Mokkapati, F. J. Beck, A. Polman, and K. R. Catchpole, "Designing periodic arrays of metal nanoparticles for light-trapping applications in solar cells," Appl. Phys. Lett. **95**(5), 053115 (2009).
22. Y. Park, E. Drouard, O. E. Daif, X. Letartre, P. Viktorovitch, A. Fave, A. Kaminski, M. Lemiti, and C. Seassal, "Absorption enhancement using photonic crystals for silicon thin film solar cells," Opt. Express **17**(16), 14312–14321 (2009).
23. J. Mayer, B. Gallinet, T. Offermans, and R. Ferrini, "Diffractive nanostructures for enhanced light-harvesting in organic photovoltaic devices," Opt. Express **24**(2), A358–A373 (2016).
24. S. C. Baker-Finch and K. R. McIntosh, "Reflection of normally incident light from silicon solar cells with pyramidal texture," Prog. Photovolt: Res. Appl. **19**(4), 406–416 (2011).
25. H. D. Omar, Md. R. Hashim, and M. Z. Pakhuruddin, "Ray tracing of inverted pyramids for light-trapping in thin crystalline silicon for solar cells," Optik **219**, 165279 (2020).
26. K. X. Wang, Z. Yu, V. Liu, Y. Cui, and S. Fan, "Absorption Enhancement in Ultrathin Solar Cells with Antireflection and Light-Trapping Nanocone Gratings," in *Renewable Energy and the Environment Optics and Photonics Congress* (OSA, 2012), p. PT2C.2.
27. L. Wen, Z. Zhao, X. Li, Y. Shen, H. Guo, and Y. Wang, "Theoretical analysis and modeling of light trapping in high efficicency GaAs nanowire array solar cells," Appl. Phys. Lett. **99**(14), 143116 (2011).
28. N. Vandamme, H.-L. Chen, A. Gaucher, B. Behaghel, A. Lemaître, A. Cattoni, C. Dupuis, N. Bardou, J.-F. Guillemoles, and S. Collin, "Ultrathin GaAs Solar Cells With a Silver Back Mirror," IEEE J. Photovolt. **5**(2), 565–570 (2015).
29. M. I. Hossain, W. Qarony, M. K. Hossain, M. K. Debnath, M. J. Uddin, and Y. H. Tsang, "Effect of back reflectors on photon absorption in thin-film amorphous silicon solar cells," Appl. Nanosci. **7**(7), 489–497 (2017).
30. V. E. Ferry, M. A. Verschuuren, H. B. T. Li, E. Verhagen, R. J. Walters, R. E. I. Schropp, H. A. Atwater, and A. Polman, "Light trapping in ultrathin plasmonic solar cells," Opt. Express **18**(S2), A237–A245 (2010).
31. Y. S. Peng and S. F. Gong, "Light-trapping structure based on ultra-thin GaAs solar cell," J. Phys. D: Appl. Phys. **53**(49), 495107 (2020).
32. Z. Cheng and D. M. O'Carroll, "Photon Recycling in Semiconductor Thin Films and Devices," Adv. Sci. **8**(20), 2004076 (2021).
33. M. Beattie, "Semiconductor Materials and Devices for High Efficiency Broadband and Monochromatic Photovoltaic Energy Conversion," Thesis, Université d'Ottawa / University of Ottawa (2021).
34. H.-L. Chen, A. Cattoni, R. De Lépinau, A. W. Walker, O. Höhn, D. Lackner, G. Siefer, M. Faustini, N. Vandamme, J. Goffard, B. Behaghel, C. Dupuis, N. Bardou, F. Dimroth, and S. Collin, "A 19.9%-efficient ultrathin solar cell based on a 205-nm-thick GaAs absorber and a silver nanostructured back mirror," Nat. Energy **4**, 761–767 (2019).

Optics EXPRESS

35. M. N. Beattie, M. Zamiri, K. L. C. Kaller, M. M. Wilkins, C. E. Valdivia, D. Xia, M. C. Tam, H. Kim, J. J. Krich, Z. Wasilewski, and K. Hinzer, "Two-Junction III-V Photonic Power Converter Operating At Monochromatic Telecom Wavelengths," in *2020 47th IEEE Photovoltaic Specialists Conference (PVSC)* (2020), pp. 1062–1066.
36. E. D. Palik, *Handbook of Optical Constants of Solids* (Academic Press, 1998), Vol. 3.
37. T. K. Chong, J. Wilson, S. Mokkapati, and K. R. Catchpole, "Optimal wavelength scale diffraction gratings for light trapping in solar cells," J. Opt. **14**(2), 024012 (2012).
38. D. Wang, D. Tan, and L. Liu, "Particle swarm optimization algorithm: an overview," Soft Comput. **22**(2), 387–408 (2018).
39. K. Ali, S. A. Khan, and M. Z. M. Jafri, "Effect of Double Layer (SiO2/TiO2) Anti-reflective Coating on Silicon Solar Cells," Int. J. Electrochem. Sci. **9**, 7865–7874 (2014).
40. C. K. Williams, T. H. Glisson, J. R. Hauser, and M. A. Littlejohn, "Energy bandgap and lattice constant contours of iii-v quaternary alloys of the form Ax By Cz D or ABx Cy Dz," J. Electron. Mater. **7**(5), 639–646 (1978).
41. T. Mei, "Interpolation of quaternary III-V alloy parameters with surface bowing estimations," J. Appl. Phys. **101**(1), 013520 (2007).
42. N. Nouri, C. E. Valdivia, M. N. Beattie, N. P. Irvin, C. Zhang, R. R. King, C. B. Honsberg, J. J. Krich, and K. Hinzer, "Tolerance Study of Thin Photonic Power Converters with Planar Back Reflectors," in *The 4th Optical Wireless and Fiber Power Transmission Conference (OWPT)* (2022).
43. N. Nouri, C. E. Valdivia, M. N. Beattie, J. J. Krich, and K. Hinzer, "Optical Design Considerations for Thin Photonic Power Converters with Textured Back Reflector," in *2022 49th IEEE Photovoltaic Specialists Conference (PVSC)* (2022).
44. N. I. Khan, S. H. Choudhury, and A. A. Roni, "A comparative study of the temperature dependence of lasing wavelength of conventional edge emitting stripe laser and vertical cavity surface emitting laser," in *Proceedings of the International Conference on Data Communication Networking and Optical Communication System* (SciTePress - Science and and Technology Publications, 2011), pp. 1–5.
45. C. E. R. Disney, S. Pillai, and M. A. Green, "The Impact of parasitic loss on solar cells with plasmonic nano-textured rear reflectors," Sci. Rep. **7**(1), 12826 (2017).
46. N. Nouri, C. E. Valdivia, M. N. Beattie, M. S. Zamiri, J. J. Krich, and K. Hinzer, "Ultrathin monochromatic photonic power converters with nanostructured back mirror for light trapping of 1310-nm laser illumination," presented at *In Physics, Simulation, and Photonic Engineering of Photovoltaic Devices X; International Society for Optics and Photonics*, Bellingham, WA, USA (2021).
47. D. Xia, M. M. Wilkins, S. S. Chahal, C. E. Valdivia, K. Hinzer, and J. J. Krich, "Opportunities for Increased Efficiency in Monochromatic Photovoltaic Light Conversion," in *2018 IEEE 7th World Conference on Photovoltaic Energy Conversion (WCPEC) (A Joint Conference of 45th IEEE PVSC, 28th PVSEC & 34th EU PVSEC)* (IEEE, 2018), pp. 3688–3692.
48. P. Sharma, A. W. Walker, J. F. Wheeldon, K. Hinzer, and H. Schriemer, "Enhanced Efficiencies for High-Concentration, Multijunction PV Systems by Optimizing Grid Spacing under Nonuniform Illumination," Int. J. Photoenergy **2014**, 1–7 (2014).
49. H. Helmers, E. Lopez, O. Höhn, D. Lackner, J. Schön, M. Schauerte, M. Schachtner, F. Dimroth, and A. W. Bett, "68.9% Efficient GaAs-Based Photonic Power Conversion Enabled by Photon Recycling and Optical Resonance," Phys. Status Solidi RRL **15**, 2100113 (2021).
50. D. Xia and J. J. Krich, "Efficiency Increase in Multijunction Monochromatic Photovoltaic Devices Due to Luminescent Coupling," J. Appl. Phys. **128**, 013101 (2020).
51. M. Levinshtein, *Handbook Series on Semiconductor Parameters* (World Scientific, 1997).
52. R. K. Ahrenkiel, R. Ellingson, S. Johnston, and M. Wanlass, "Recombination lifetime of In0.53Ga0.47As as a function of doping density," Appl. Phys. Lett. **72**, 3470–3472 (1998).
53. B. L. Smith, Z. S. Bittner, S. D. Hellstroem, G. T. Nelson, M. A. Slocum, A. G. Norman, D. V. Forbes, and S. M. Hubbard, "InAlAs photovoltaic cell design for high device efficiency," Prog. Photovolt: Res. Appl. **25**, 706–713 (2017).